Emergent Spatial Coordination from Negative Selection Alone: The Role of Observation Richness in Objective-Free Artificial Life

Anonymous

Abstract

We show that spatial coordination among agents emerges in a multi-agent grid world when agents can observe neighbor states, without any objective function guiding the search. Existing artificial life systems typically rely on fitness functions—explicit or implicit—which introduce evaluation bias and constrain the space of discoverable phenomena. We propose an objective-free approach based on large-scale random rule generation with physical-inconsistency-only filtering, comparing four observation conditions: random walk, a step-clock control, density-only observation, and state-profile observation. Across 5,000 rules per condition, agents with state-profile observation achieve nonzero median excess MI (MI calibrated by a permutation-based shuffle null that controls for pair-count bias) while density-only and control agents remain at zero (Cliff's $\delta = 0.34$; median-difference bootstrap 95% CI $[0.26, 0.30]$; Table 2), and the evidence ladder Control $\leq$ Phase 1 $<$ Phase 2 holds across all rule-based comparisons. A Miller-Madow bias-corrected estimator is used throughout, and a shuffle null confirms that the random walk's elevated raw MI is entirely attributable to pair-count bias ($\mathrm{MI}_{\mathrm{excess}} \approx 0$). Moran's I further distinguishes local coordination from large-scale clustering. These results demonstrate that observation channel richness—not rule table capacity or selection pressure—drives the emergence of spatial coordination in objective-free systems.

1 Introduction

Artificial life research aims to understand the principles of living systems by constructing synthetic analogs (Bedau, 2003). A recurring challenge is the role of the *objective function*: most evolutionary and adaptive systems require an explicit fitness measure that guides search toward "interesting" configurations. Even novelty search (Lehman and Stanley, 2011), which abandons traditional fitness, still uses a novelty metric as an implicit objective.

This reliance on objectives introduces a subtle but pervasive bias. The choice of fitness function constrains which phenomena can emerge, and researchers may inadvertently encode their expectations into the evaluation criteria (Stanley et al., 2019). The question then arises: *can meaningful spatial structure emerge in a multi-agent system with no fitness function?*

We explore the unexplored quadrant of *no objective* × *selection pressure*, where the only filtering criterion is physical consistency—removing rules that produce trivially broken simulations (all agents halt or converge to a single state). This minimal filtering is analogous to the laws of physics: it constrains what is possible without specifying what is desirable.

Our core contribution is threefold:

1. A minimal grid-world model with objective-free negative selection, where random rule tables are evaluated and only physically inconsistent ones are discarded.

2. Evidence that *observation richness*—the amount of neighbor state information available to agents—drives emergent spatial coordination, independent of rule table capacity.

3. Robustness across four experimental conditions and 20,000 rule evaluations, with statistical significance confirmed by Mann-Whitney U tests with Holm-Bonferroni correction.

2 Related Work

Self-organization without selection. Cellular automata such as Conway's Game of Life (Gardner, 1970) and Wolfram's elementary rules (Wolfram, 1984) demonstrate that simple local rules can produce complex global patterns. Continuous extensions like Lenia (Chan, 2019) show rich morphogenetic dynamics in continuous state spaces. Reynolds' Boids (Reynolds, 1987) produce flocking behavior from three local rules. These systems share a common trait: the rules are hand-designed, not discovered through search.

Evolutionary ALife with fitness. Tierra (Ray, 1991) and Avida (Ofria and Wilke, 2004) use implicit fitness through resource competition and self-replication. While these systems produce open-ended dynamics, the replication criterion itself acts as a fitness function that selects for self-replicating programs.

Novelty search and open-endedness. Novelty search (Lehman and Stanley, 2011, 2008) replaces fitness with a novelty metric, enabling discovery of diverse behaviors. The open-ended evolution community has explored various approaches to sustaining innovation (Taylor et al., 2016; Stanley et al., 2019). However, all such approaches still employ an evaluation function—whether fitness, novelty, or complexity.

Information-theoretic measures. Mutual information and transfer entropy have been used to quantify coordination in multi-agent systems (Lizier et al., 2012). We use mutual information as a *post-hoc* analysis tool, never as a selection criterion.

Our position. Our approach differs from all the above by using *no* evaluation function —not fitness, not novelty, not complexity. We generate random rules, discard only physically broken ones, and ask what structure the surviving rules exhibit.

3 Methods

3.1 World Model

The simulation environment is a 20×20 toroidal grid populated by 30 agents (Figure 1). Each agent occupies exactly one cell (no overlap allowed) and maintains an internal state $s \in \{0, 1, 2, 3\}$. At each of 200 time steps, agents are updated in a random sequential order: one agent at a time observes its local neighborhood, looks up an action in a shared rule table, and executes it. The action space comprises 9 mutually exclusive actions: 4 cardinal movements, 4 state changes, and a no-op. Movement to an occupied cell fails silently.

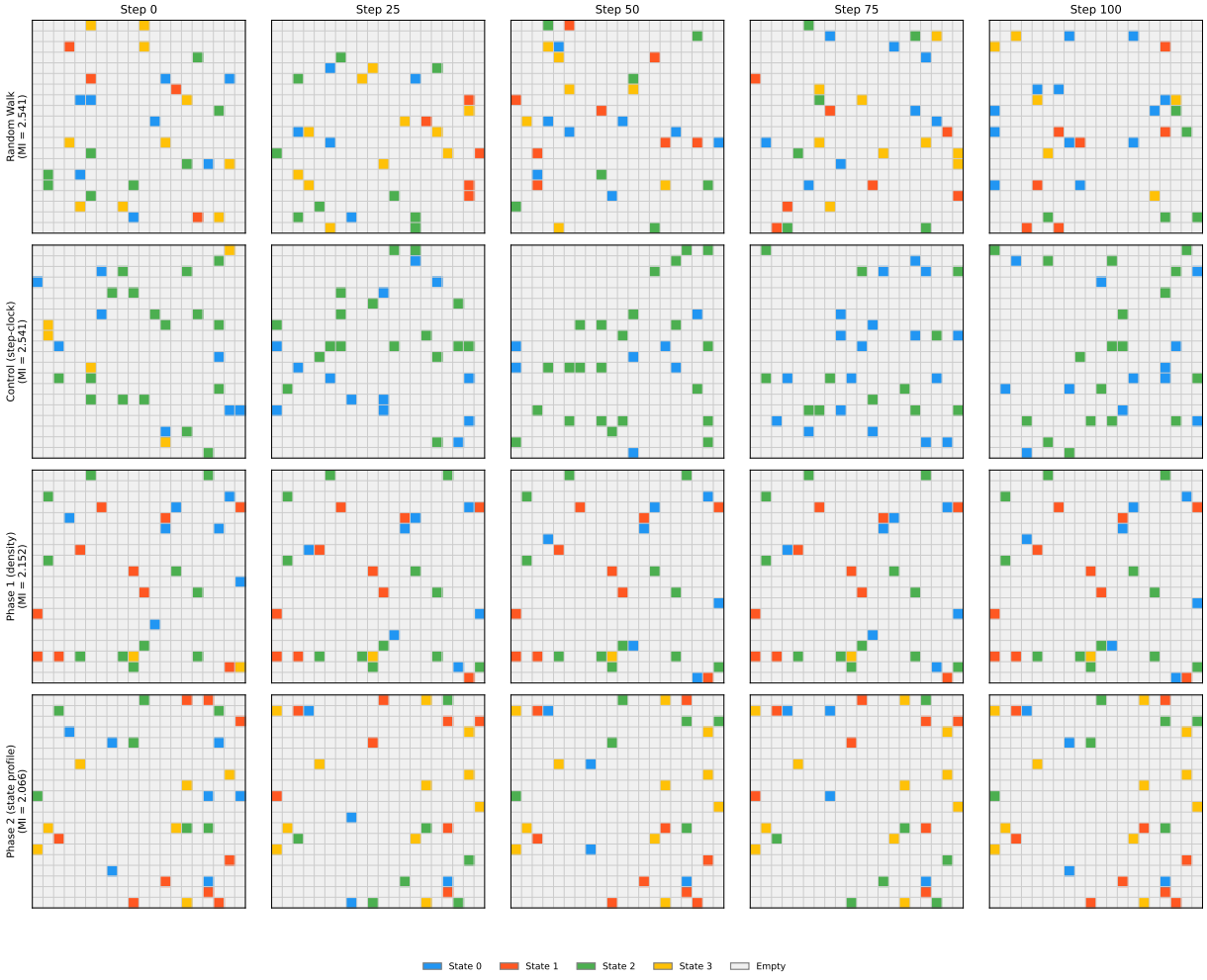

Figure 1: Grid snapshots of representative rules from each condition. Each panel shows the 20×20 toroidal grid with agents colored by internal state. Phase 2 rules produce visibly clustered spatial patterns, while Control rules appear disordered.

3.2 Observation Phases

We compare four observation conditions that vary in the information available to agents:

Random Walk (RW). Each agent selects an action uniformly at random from $\{0, \ldots, 8\}$ at every step, ignoring the rule table entirely. This baseline isolates the contribution of grid geometry (collision avoidance, toroidal wrapping) from rule-driven behavior, and also serves to calibrate the MI estimator under conditions with minimal spatial clustering.

Control (step-clock). Agents observe their own state $s \in \{0, \ldots, 3\}$, the count of occupied von Neumann neighbors $n \in \{0, \ldots, 4\}$, and a periodic step clock $t \bmod 5 \in \{0, \ldots, 4\}$. The rule table has $4 \times 5 \times 5 = 100$ entries. The step clock provides no neighbor state information—it is a non-informative third dimension that matches the table size of Phase 2 without adding spatial content.

Phase 1: density-only (P1). Agents observe their own state s and neighbor count n. The rule table has $4 \times 5 = 20$ entries, indexed by $5s + n$. This is the minimal observation that couples agents spatially.

Phase 2: state profile (P2). Agents observe their own state s, neighbor count n, and the dominant neighbor state $d \in \{0, \ldots, 4\}$ (the most frequent state among occupied neighbors, with ties broken by smallest value; 4 denotes no occupied neighbors). The rule table has $4 \times 5 \times 5 = 100$ entries, indexed by $25s + 5n + d$.

3.3 Physical Filters

Only two filters are applied, both targeting physical inconsistency rather than behavioral quality:

- **Halt detection**: If all agents' positions and states remain unchanged for 10 consecutive steps, the simulation is terminated early.
- **State uniformity**: If all 30 agents converge to the same internal state, the simulation is terminated (an indistinguishable system is information-theoretically trivial).

No fitness function, novelty metric, complexity threshold, or behavioral criterion is used at any stage.

3.4 Metrics

All metrics are computed post-hoc and never used for selection:

Neighbor mutual information (MI). For each pair of adjacent occupied cells (i, j) on the toroidal grid, we compute the mutual information between their internal states:

$$I(S_i; S_j) = \sum_{s_i, s_j} p(s_i, s_j) \log_2 \frac{p(s_i, s_j)}{p(s_i)\, p(s_j)} \tag{1}$$

where the joint and marginal distributions are estimated from all adjacent occupied pairs at a given time step. To mitigate the positive bias of the plug-in estimator at small sample

sizes, we apply the Miller-Madow correction (Miller, 1955): $\hat{I}_{\text{MM}} = \hat{I} - (K_{\text{joint}} - K_X - K_Y + 1)/(2n \ln 2)$, where K_{joint}, K_X, and K_Y are the counts of non-zero bins in the joint and each marginal distribution respectively, and n is the number of pairs. Values are clamped to ≥ 0. High MI indicates that neighboring agents' states are statistically dependent—a signature of spatial coordination.

Shuffle-null MI calibration. To control for pair-count bias—where configurations with few neighbor pairs produce inflated MI estimates regardless of state structure—we compute a permutation-based shuffle null. For each rule's final snapshot, we fix occupied positions and randomly reassign states among them $N = 200$ times, computing $\hat{I}_{\text{MM}}$ for each shuffle. The mean across shuffles is the shuffle-null MI. The *excess MI*, $\text{MI}_{\text{excess}} = \hat{I}_{\text{MM}} - \overline{I}_{\text{shuffle}}$, isolates genuine spatial coordination from estimation artifacts. In particular, the random walk's high raw MI (≈ 0.36 bits) is entirely attributable to pair-count bias: $\text{MI}_{\text{excess}} \approx 0$.

Moran's I. Spatial autocorrelation is quantified by Moran's I across occupied cells using torus 4-neighborhood weights: both cells must be occupied for a weight of 1. Values range from -1 (dispersed) through 0 (random) to $+1$ (clustered). Moran's I provides an independent confirmation that elevated MI reflects genuine spatial clustering, not a statistical artifact.

State entropy. Shannon entropy of the internal state distribution across all agents: $H = -\sum_s p(s) \log_2 p(s)$.

Action entropy. Per-agent Shannon entropy of the cumulative action distribution, summarized as the mean and variance across agents.

3.5 Experimental Design

For each of the four conditions, we generate 5,000 random rule tables using deterministic seeds (rule seeds 0–4,999, simulation seeds 0–4,999). Each rule table is evaluated on a single 200-step simulation. Surviving rules (those not terminated by halt or state-uniformity filters) have their final-step metrics recorded.

Statistical comparisons use two-sided Mann-Whitney U tests (Mann and Whitney, 1947) with Holm-Bonferroni correction (Holm, 1979) applied across all metrics within each pairwise comparison. Each pairwise comparison (e.g., P1 vs. P2) tests a distinct hypothesis about the effect of observation content, so correction is applied per comparison rather than globally across all stages. Effect sizes are reported as Cliff's δ (equivalent to rank-biserial correlation for Mann-Whitney U): $\delta = 1 - 2U_A/(n_1 n_2)$, where U_A is the U statistic for the first-listed group. To replace extreme p-values with more informative measures, we report bootstrap 95% confidence intervals for the median difference (10,000 resamples, percentile method) as the primary effect-size statistic; p-values are retained as secondary evidence. Each rule table is paired with a single simulation seed (rule seed i paired with simulation seed i), so per-rule conclusions reflect one initial configuration.

4 Results

4.1 Evidence Ladder Among Rule-Based Conditions

Table 1 and Figure 2 present the neighbor mutual information across all four conditions. Among the three rule-based conditions, a clear monotonic ordering emerges:

Control < Phase 1 < Phase 2

Table 1: Neighbor mutual information and spatial clustering by condition. MI values use the Miller-Madow bias-corrected estimator; $\text{MI}_{\text{excess}} = \text{MI}_{\text{observed}} - \text{MI}_{\text{shuffle null}}$ controls for pair-count bias (5,000 rules per condition, $N = 200$ shuffles). The random walk's high raw MI is entirely attributable to pair-count bias ($\text{MI}_{\text{excess}} \approx 0$).

Condition	Table Size	Median MI	Median $\text{MI}_{\text{excess}}$	Median Moran's I	Survival
Random Walk	1 (unused)	0.910	0.050	−0.030	100.0%
Control	100	0.000	0.000	0.124	44.5%
Phase 1	20	0.019	0.000	−0.011	71.4%
Phase 2	100	0.298	0.096	−0.020	74.7%

The control condition, despite having 100-entry tables (equal to Phase 2), produces zero median excess MI—demonstrating that table size alone is insufficient. Phase 2 is the only rule-based condition with nonzero median excess MI, driven by access to neighbor state information (Table 2; bootstrap 95% CI excludes zero).

4.2 Random Walk Baseline and Shuffle-Null Calibration

All MI values in this paper use the Miller-Madow bias-corrected estimator (Miller, 1955), which subtracts a first-order correction term from the naive plug-in estimate. However, this correction becomes insufficient when the number of neighbor pairs n is comparable to the number of joint-distribution bins K—precisely the regime of random-walk agents, where ≈4–5 adjacent pairs populate up to 16 joint categories.

The shuffle null resolves this directly. By permuting states among fixed positions ($N = 200$ shuffles per rule), we obtain the expected MI under the null hypothesis of no spatial state structure. The excess MI ($\text{MI}_{\text{excess}} = \text{MI}_{\text{observed}} - \overline{\text{MI}}_{\text{shuffle}}$) isolates genuine coordination from pair-count artifacts.

For the random walk, $\text{MI}_{\text{excess}} \approx 0$ (Table 1), confirming that its elevated raw MI is entirely attributable to pair-count bias—not spatial structure. In contrast, Phase 2 retains substantial excess MI, demonstrating genuine coordination that persists after bias calibration. Notably, the Control condition—not Phase 2—has the highest median Moran's I (0.124), reflecting clustered but uncoordinated spatial patterns from its large table size. Phase 2's median Moran's I (−0.020) is near zero, indicating that its elevated MI arises from local state coordination among neighbors rather than from large-scale spatial clustering.

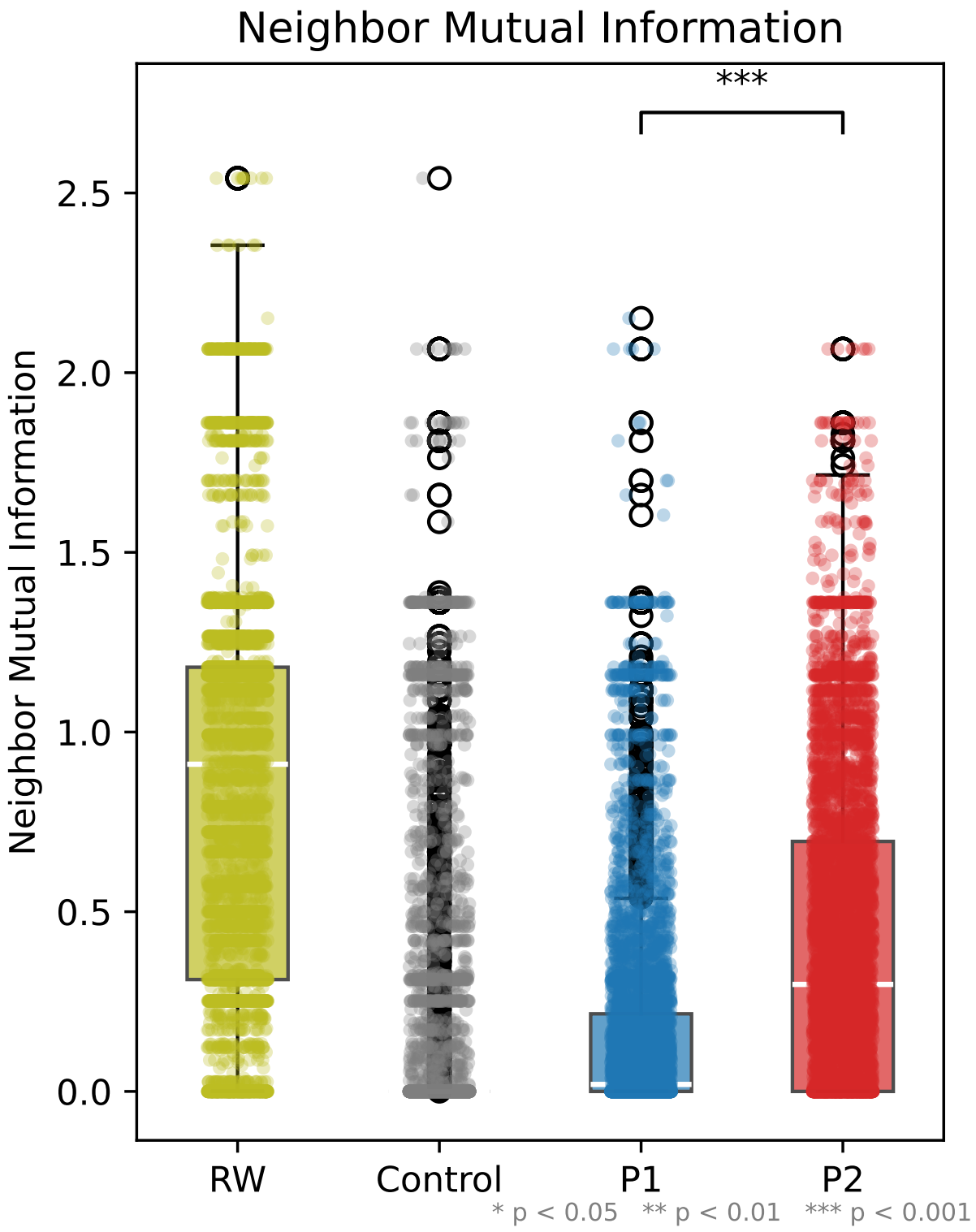

Figure 2: Neighbor mutual information distributions across rule-based conditions. Box plots with scatter strips show the full distribution of final-step MI values for surviving rules. The evidence ladder Control < P1 < P2 is clearly visible.

The random-walk baseline remains informative: it validates the shuffle-null calibration procedure, establishes the bias floor, and confirms that all 5,000 random-walk rules survive (100% survival rate) since random actions never trigger halt or state-uniformity filters.

4.3 Table-Size Confound Resolved

A natural objection is that Phase 2's higher MI could result from its larger rule table (100 entries vs. 20 for Phase 1), which permits more complex behaviors. The control condition resolves this confound directly: it uses 100-entry tables—identical in size to Phase 2—but replaces the informative dominant-neighbor-state dimension with a non-informative step clock. The control produces *lower* MI than Phase 1 despite having 5× more table entries. This demonstrates that **observation content, not table capacity, drives emergent coordination**.

The pairwise comparisons confirm this (Table 2): Phase 1 produces significantly higher MI than Control despite having smaller tables, and Phase 2 vastly exceeds Control despite equal table size.

4.4 Temporal Dynamics

The four conditions exhibit qualitatively distinct temporal behaviors (Figure 3):

- **Phase 1**: MI rises quickly then plateaus—"frozen" dynamics where spatial patterns crystallize early.
- **Phase 2**: MI rises and remains dynamic, with ongoing fluctuations—sustained spatial coordination without freezing.
- **Control**: Highly chaotic trajectories with large MI variance and frequent collapses to zero.
- **Random Walk**: High but flat MI throughout, reflecting constant estimation bias from few adjacent pairs rather than genuine coordination.

This pattern is suggestive of an edge-of-chaos interpretation (Langton, 1990; Packard, 1988): Phase 1 falls into frozen order, Control produces undirected chaos, and Phase 2 occupies an intermediate regime where coordination persists dynamically. However, this observation is based on a small sample of top-performing rules per condition and lacks quantitative measures of criticality (e.g., Lyapunov exponents); we note it as a qualitative pattern rather than a strong claim.

4.5 Statistical Significance

Table 2 presents Mann-Whitney U test results for the primary metric (neighbor MI) across all pairwise comparisons. All comparisons are highly significant after Holm-Bonferroni correction.

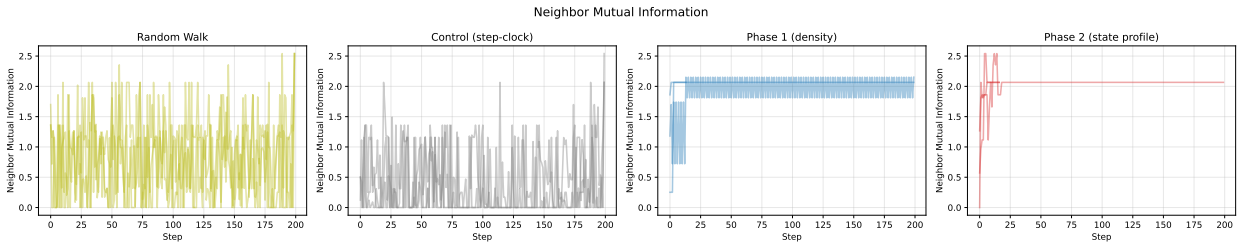

Figure 3: MI time-series trajectories for top-3 rules per condition. Phase 1 freezes early, Phase 2 remains dynamic, and Control shows chaotic fluctuations.

Table 2: Pairwise statistical tests for neighbor MI. Effect sizes are Cliff's δ (= rank-biserial r). Bootstrap 95% CIs for the median difference (10,000 resamples) are the primary effect-size statistic; p-values (Holm-Bonferroni corrected) are secondary.

Comparison	Direction	Cliff's δ	Median diff 95% CI	p-value
P1 vs. P2	P2 > P1	0.339	[0.260, 0.295]	$< 10^{-199}$
P1 vs. Control	P1 > Ctrl	0.270	[0.012, 0.026]	$< 10^{-158}$
Control vs. P2	P2 > Ctrl	0.482	[0.281, 0.311]	≈ 0

4.6 Survival Analysis

Survival rates differ significantly across conditions (Table 1). Phase 2 achieves the highest survival rate, followed by Phase 1 and Control. State-uniformity is the dominant termination mode for the control condition, suggesting that without neighbor state information, rules frequently drive all agents to the same state.

5 Discussion

Observation richness as a driver of emergence. Our central finding is that the *content* of observation—specifically, access to neighbor state information—is the primary driver of emergent spatial coordination. This holds even when controlling for rule table size (the control condition). With shuffle-null-calibrated MI, Phase 2 is the only rule-based condition achieving nonzero median excess MI, while both Phase 1 and Control fall to zero—making the qualitative separation between observation conditions unambiguous. Moran's I reveals that the Control condition exhibits the strongest spatial clustering (median $I = 0.124$) despite zero excess MI, while Phase 2's near-zero median I (-0.020) indicates that its coordination operates at the local neighbor level rather than through large-scale spatial clustering. This result is not a consequence of having more rules to choose from, but of each rule being able to respond to richer local information.

Edge-of-chaos interpretation. The temporal dynamics are suggestive of a connection to the edge-of-chaos hypothesis (Langton, 1990). Phase 1's frozen dynamics and Control's chaotic behavior bracket Phase 2, which maintains dynamic spatial coordination without col-

lapsing into static patterns. This qualitative observation—based on top-performing rules—warrants future investigation with quantitative criticality measures.

Remove broken, observe survivors. Our methodology embodies a minimal philosophy: generate random configurations, remove only the physically broken ones, and examine what structure the survivors exhibit. This "negative selection" approach avoids the evaluation bias inherent in fitness-driven search. The surprising finding is that meaningful structure—quantified by mutual information—emerges even under this minimal regime, provided the observation channel is sufficiently rich.

Implications for ALife research. These results suggest that objective-free search deserves more attention as a complement to fitness-driven approaches. When the goal is to discover *what is possible* rather than to optimize for a specific outcome, removing the objective function may reveal phenomena that fitness landscapes obscure. The key enabler is not the search algorithm but the *architecture* of the agents—specifically, what they can observe.

6 Limitations

Several limitations constrain the generalizability of our findings:

- **Single topology**: All experiments use a 20×20 toroidal grid with von Neumann neighborhoods. Other topologies (hexagonal grids, Moore neighborhoods, irregular graphs) may produce different results.
- **Symmetric metric**: Mutual information is symmetric and measures correlation, not causation. Transfer entropy would provide directional information flow but was not computed in this study.
- **No multi-generation evolution**: Each rule table is evaluated in a single 200-step simulation. We do not evolve rules across generations, which limits comparison with evolutionary ALife systems.
- **Small state space**: With only 4 internal states and 9 actions, the model is deliberately minimal. Scaling to larger state spaces may reveal qualitatively different dynamics.
- **Density fixed**: The main experiments use 30 agents on a 400-cell grid (7.5% density). Appendix A reports a systematic density sweep across 12 conditions (density range 0.017–0.400), confirming that the Phase 2 MI advantage holds across all tested densities.
- **Sequential update order**: Agents are updated in a random permutation each step, creating implicit temporal correlations between early and late updates within the same step. Synchronous update schemes may produce different dynamics.
- **Single simulation per rule**: Each rule table is evaluated with a single initial configuration (rule seed i paired with simulation seed i). Stochastic variation across different initial configurations for the same rule is not explored.

7 Conclusion

We have shown that meaningful spatial coordination emerges in a multi-agent system through objective-free negative selection, and that the richness of agents' observation channels—not rule table capacity—is the critical factor. The evidence ladder from step-clock control through density-only to state-profile observation demonstrates a monotonic relationship between observation content and emergent coordination, confirmed by a bias-corrected MI estimator across all tested density levels (Appendix A).

Future work should investigate directional information flow using transfer entropy, extend to larger grids and state spaces, and explore multi-generation rule evolution under the same objective-free regime. The broader implication is that the "remove broken, observe survivors" philosophy can serve as a productive complement to fitness-driven search in artificial life.

A Density Sweep Robustness

The main experiments use a fixed density of 7.5% (30 agents on a 20×20 grid). To assess robustness across density levels, we evaluated both Phase 1 and Phase 2 across 12 density conditions: 3 grid sizes (15×15, 20×20, 30×30) $\times$ 4 agent counts (15, 30, 60, 90), yielding densities from 0.017 to 0.400. Each condition was evaluated with 600 rules (100 rules $\times$ 6 seed batches), totaling 14,400 rule evaluations, all using the Miller-Madow bias-corrected MI estimator.

Table 3: Density sweep results across 12 conditions. Phase 2 achieves nonzero median MI in 8 of 12 conditions, including all conditions with ≥ 60 agents, while Phase 1 remains at zero across all densities tested.

Density	Grid	Agents	Median MI (bits)		Survival (%)	
			P1	P2	P1	P2
0.017	30×30	15	0.000	0.000	86.7	86.7
0.033	30×30	30	0.000	0.000	83.3	85.8
0.037	20×20	15	0.000	0.000	80.8	81.8
0.067	15×15	15	0.000	0.000	68.7	76.0
0.067	30×30	60	0.000	0.167	70.5	76.3
0.075	20×20	30	0.000	0.106	70.2	72.5
0.100	30×30	90	0.000	0.217	67.0	74.2
0.133	15×15	30	0.000	0.129	62.2	64.8
0.150	20×20	60	0.000	0.180	63.0	69.7
0.225	20×20	90	0.000	0.154	64.0	76.7
0.267	15×15	60	0.000	0.121	63.5	72.7
0.400	15×15	90	0.000	0.088	68.0	83.7

Table 3 and Figures 4 and 5 present the results. Phase 2 achieves nonzero median MI in 8 of 12 conditions, including all conditions with ≥ 60 agents, peaking near $d = 0.100$ (MI

= 0.217 bits at 30 × 30, 90 agents) before declining at higher densities. Phase 1 remains at zero median MI across all 12 conditions, confirming that the Phase 2 advantage is not an artifact of the specific grid configuration used in the main experiments.

Phase 2 also consistently achieves higher survival rates than Phase 1, with the gap widening at higher densities (e.g., 76.7% vs. 64.0% at $d = 0.225$; 83.7% vs. 68.0% at $d = 0.400$).

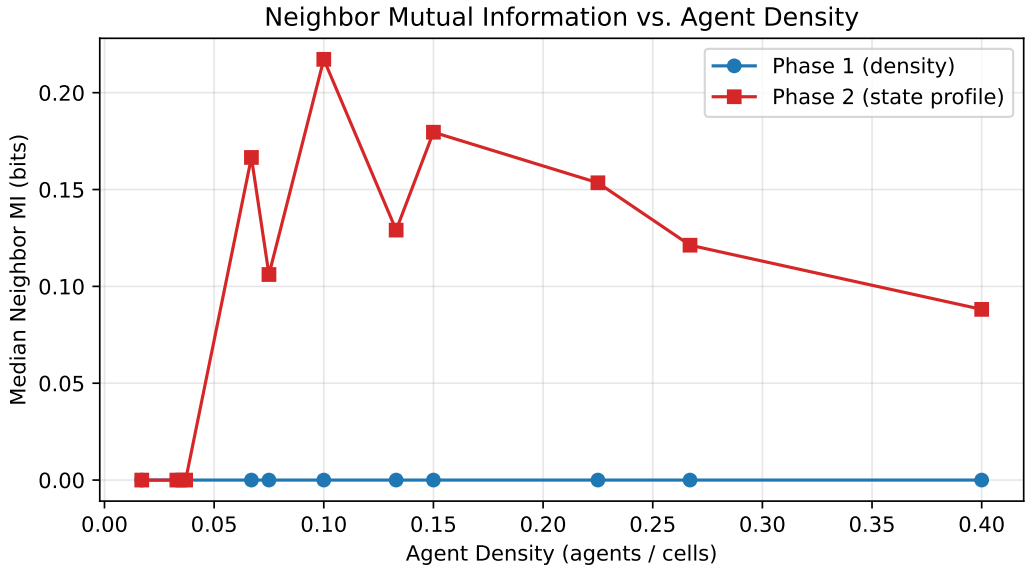

Figure 4: Median neighbor MI vs. agent density for Phase 1 and Phase 2. Phase 2 MI peaks at medium densities and declines at higher densities, while Phase 1 remains at zero throughout.

References

Bedau, M. A. (2003). Artificial life: Organization, adaptation and complexity from the bottom up. *Trends in Cognitive Sciences*, 7(11):505–512.

Chan, B. W.-C. (2019). Lenia: Biology of artificial life. *Complex Systems*, 28(3):251–286.

Gardner, M. (1970). Mathematical games: The fantastic combinations of John Conway's new solitaire game "life". *Scientific American*, 223(4):120–123.

Holm, S. (1979). A simple sequentially rejective multiple test procedure. *Scandinavian Journal of Statistics*, 6(2):65–70.

Langton, C. G. (1990). Computation at the edge of chaos: Phase transitions and emergent computation. *Physica D: Nonlinear Phenomena*, 42(1–3):12–37.

Lehman, J. and Stanley, K. O. (2008). Exploiting open-endedness to solve problems through the search for novelty. In *Proceedings of the Eleventh International Conference on Artificial Life (ALIFE XI)*, pages 329–336.

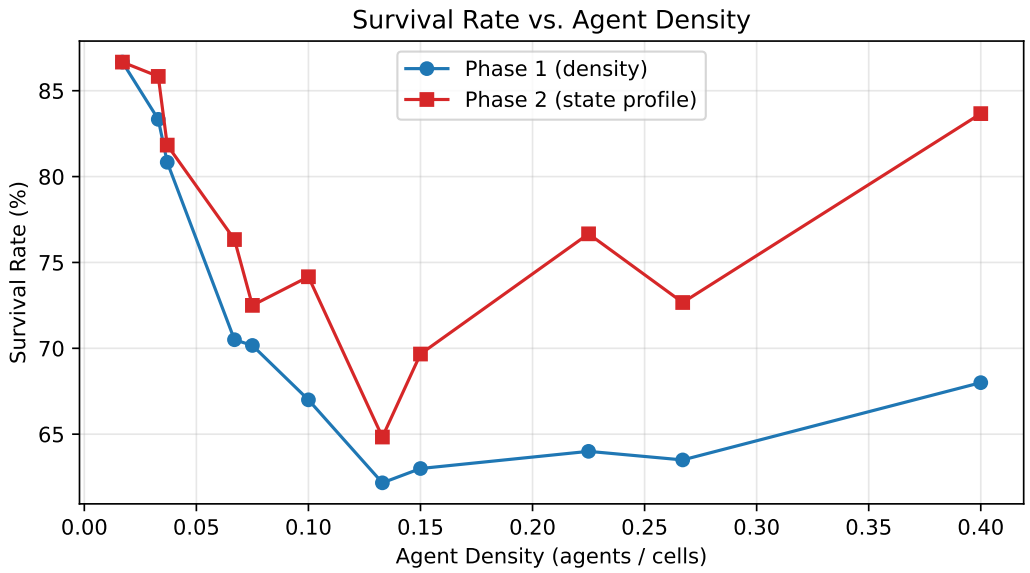

Figure 5: Survival rate vs. agent density. Phase 2 consistently achieves higher survival than Phase 1, with the gap widening at higher densities.

Lehman, J. and Stanley, K. O. (2011). Abandoning objectives: Evolution through the search for novelty alone. *Evolutionary Computation*, 19(2):189–223.

Lizier, J. T., Prokopenko, M., and Zomaya, A. Y. (2012). Local measures of information storage in complex distributed computation. *Information Sciences*, 208:39–54.

Mann, H. B. and Whitney, D. R. (1947). On a test of whether one of two random variables is stochastically larger than the other. *The Annals of Mathematical Statistics*, 18(1):50–60.

Miller, G. A. (1955). Note on the bias of information estimates. In Quastler, H., editor, *Information Theory in Psychology: Problems and Methods*, pages 95–100. Free Press, Glencoe, IL.

Ofria, C. and Wilke, C. O. (2004). Avida: A software platform for research in computational evolutionary biology. *Artificial Life*, 10(2):191–229.

Packard, N. H. (1988). Adaptation toward the edge of chaos. In *Dynamic Patterns in Complex Systems*, pages 293–301.

Ray, T. S. (1991). An approach to the synthesis of life. In Langton, C. G., Taylor, C., Farmer, J. D., and Rasmussen, S., editors, *Artificial Life II*, pages 371–408. Addison-Wesley.

Reynolds, C. W. (1987). Flocks, herds and schools: A distributed behavioral model. In *Proceedings of the 14th Annual Conference on Computer Graphics and Interactive Techniques (SIGGRAPH '87)*, pages 25–34. ACM.

Stanley, K. O., Lehman, J., and Soros, L. (2019). Why open-endedness matters. *Artificial Life*, 25(2):33–42.

Taylor, T., Bedau, M., Channon, A., Ackley, D., Banzhaf, W., Beslon, G., Dolson, E., Froese, T., Hickinbotham, S., Ikegami, T., McMullin, B., Packard, N., Rasmussen, S., Virgo, N., Agmon, E., Clark, E., McGregor, S., Ofria, C., Ropella, G., Spector, L., Stanley, K. O., Stanton, A., Timperley, C., Vostinar, A., and Wiser, M. (2016). Open-ended evolution: Perspectives from the OEE workshop in York. *Artificial Life*, 22(3):408–423.

Wolfram, S. (1984). Cellular automata as models of complexity. *Nature*, 311(5985):419–424.